Available online at www.sciencedirect.com
SCIENCE DIRECT®
Journal of Power Sources 134 (2004) 57–71
JOURNAL OF POWER SOURCES
www.elsevier.com/locate/jpowsour

The scaling behavior of flow patterns: a model investigation

S.W. Cha [a,*], R. O'Hayre [b], Y. Saito [a], F.B. Prinz [a,b]

[a] *Department of Mechanical Engineering, Stanford University, Stanford, CA 94305, USA*
[b] *Department of Material Science and Engineering, Stanford University, Stanford, CA 94305, USA*

Received 11 February 2004; accepted 10 March 2004

Available online 1 Jun 2004

Abstract

Fuel cell flow channel scaling behavior has been investigated for three different flow pattern archetypes (interdigitated, serpentine, and spiral interdigitated) by employing computational fluid dynamics (CFD). The range of investigation covers flow channels of macro feature size (>500 μm) to micro feature size (<100 μm). Each flow pattern archetype exhibits unique scaling behavior. For most flow pattern archetypes, optimal feature size occurs at an intermediate channel dimension. Extremely small flow channels do not optimize performance despite improved mass transport. Pressure drop loss and flow travel path in the cathode compartment are major factors determining the optimal size. The scaling phenomena are explained in conjunction with the details of oxygen distribution in the cathode flow channels and gas diffusion layer.

Keywords: Fuel cells; PEMFC; Micro flow channels; CFD

1. Introduction

Miniature fuel cells are drawing increasing attention as a possible solution for improved power sources for portable power systems [1–4]. Recently, the adaptation of micro fabrication technology has enabled the generation of successful prototypes [5–10] Also, components employed in such prototypes—e.g. thin film catalyst, and micro flow channels—have been characterized systematically regarding their effect on overall fuel cell performance [8–11].

In past decades, numerous fuel cell modeling studies have successfully integrated the electrochemical reactions and the transport phenomena with CFD [12–20]. Moreover, some of these efforts have demonstrated the capability of addressing three-dimensional fuel cell geometries [17–20].

Recently, we have explored the transport phenomena of microscale parallel flow channels theoretically and experimentally [8–10]. The work presented in this paper extends the CFD model investigation of flow channels to three other types of flow patterns: interdigitated, serpentine, and spiral-interdigitated flow channels. The investigation results of the scaling effect of these flow geometries ranging from micro scale to macro sale will be discussed.

2. Investigation on size scaling of flow channels

In general, fuel cell performance improves as the channel gas flow velocity increases since the increased flow velocity enhances convective mass transport [21]. During actual fuel cell operation, the flow tends to be wasted beyond the stoichiometric condition if no downstream system components such as an afterburner consume the unused fuel and oxidant. Thus, increasing flow velocity is a challenging task if it entails wasted flow or the power consumption of an auxiliary device, such as a pump.

However, when flow channels with smaller cross-section are employed in fuel cells, the flow velocity can be increased while maintaining a constant gas stoichiometric number. Accordingly, we may expect fuel cell performance improvements at little additional cost.

However, the investigation of the scaling effect of flow channels is a daunting task considering the number of geometric parameters involved with flow channels: the flow channel pattern, the channel and rib shape, and the diffusion layer thickness, among others. Therefore, it is neces-

* Corresponding author. Tel.: +1-650-736-0275; fax: +1-650-723-5034.
E-mail address: swcha@stanford.edu (S.W. Cha).

0378-7753/$ – see front matter © 2004 Elsevier B.V. All rights reserved.
doi:10.1016/j.jpowsour.2004.03.036

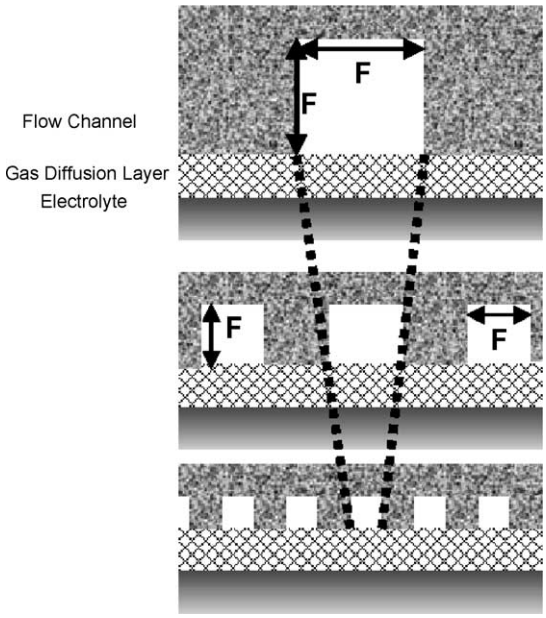

Fig. 1. The scaling scheme of flow channels associating only one "feature size", *F*. The total cross-sectional area of flow channels is directly proportional to the feature size.

sary to dramatically reduce the number of parameters without sacrificing the range of investigation. One simple solution for meeting this requirement would be to confine the cross-sectional shape of the flow channels to a certain geometry, such as a square. A square has only *one* geometric parameter, the length of one of its sides. Moreover, if the dividing ribs employ the same square shapes as the flow channels, the entire flow channel pattern can be represented by that single geometric parameter. This parameter can be defined as the feature size. Fig. 1 depicts the idea of feature size, *F*.

The operating conditions of the fuel cell are described by several parameters too, such as the stoichiometric ratio of the reactants, cell temperature, and the humidity of reactant gases. As stated earlier, these parameters must remain constant for a fair comparison of performance at each feature size. Please note that under constant gas stoichiometry conditions, small channels accommodate faster gas flow than large channels, with the gas velocity proportional to the inverse of the feature size, as explained in Eqs. (1) and (2) below

$$N = AV = nA_{\mathrm{i}}V = \text{constant} \tag{1}$$

where N, A, V, n, A_{i} stand for the total volumetric flow rate, the total cross-sectional area of the flow channels, the flow velocity, the number of flow channels, and the individual cross-sectional area of each flow channel, respectively. From Fig. 1, it is clear that n is inversely proportional to feature size, F, and A_{i} are proportional to the square of F. Thus, from Eq. (1)

$$V = \frac{N}{nA_{\mathrm{i}}} \sim \frac{N}{(1/F)F^2} \sim \frac{N}{F} \tag{2}$$

Thus, we can see that the velocity in the flow channel will *increase* as the feature size *decreases*. An increase in gas velocity will facilitate reactant delivery to reaction sites by improved convection. Moreover, a dramatic improvement can be expected regarding the efficiency with which products are removed from the reaction sites. This is particularly important because the voltage drop due to the product's occupation of reaction sites is a significant percentage of the total voltage losses, especially at high current densities [22].

One drawback of the smaller feature size is the increased pressure drop in the flow channels. However, considering that microchannels would likely be adapted for miniature fuel cells, the actual pressure drop may still small since the absolute length scale is relatively short in miniature fuel cells. We will discuss the effect of feature size scaling on the cell performance in conjunction with the pressure drop in this paper.

3. Model development

The electrochemical reactions in a fuel cell involve various transport phenomena including the dissociation and association of molecules, ions and electrons. Furthermore, liquid water generation on the cathode side adds the complexity of two-phase flow especially in PEM fuel cells. Thus, the modeling of a fuel cell system requires a certain idealization of the true situation.

3.1. Model assumptions

In the fuel cell models created for this study, the following common simplifying assumptions are made. (Please refer to similar assumptions in previous computational studies [12,15,17].)

1. The gas mixture is ideal.
2. Fuel cells operate at steady state.
3. Laminar flow is assumed.
4. Water can exist only in the vapor phase.
5. The ionic conductivity of the membrane is assumed to be constant regardless of the humidification level. Also, no water flux exists across the membrane.
6. The membrane is impermeable to the reactant and product gases.
7. An isothermal condition is assumed for the entire computational domain.
8. The effects of gravity are ignored.
9. The ionic distribution and the electric field in the membrane phase are neglected.

Table 1
The physical dimensions of fuel cell models

Quantity	Value
Active area length, L (mm)	14
Active area width, W (mm)	14
Feature size, F (μm)	5, 20, 50, 100, 200, 500, 1000 (interdigitated channels) 99, 203, 483 (serpentine channels) 101, 209, 510 (spiral-interdigitated channels)
Gas diffusion layer thickness, t_g (mm)	0.25
Catalyst thickness, t_c (mm)	0.05
Membrane thickness, t_m (mm)	0.125
Flow inlet (or outlet) length, L_i ($=L_o$) (mm) (interdigitated channels only)	1

3.2. Governing equations

A single set of governing equations has been employed for all computational domains, similar to the approaches of Um et al. [15] and Gurau et al. [12]. The details of the governing equations are described elsewhere [23].

3.3. Physical parameters

All models of different feature sizes and flow patterns share similar geometric constraints and physical conditions. All models share 14 mm × 14 mm (2 cm^2) active area dimensions, and the same thickness of gas diffusion layer, catalyst, and membrane geometry. The physical dimensions of the model geometries are summarized in Table 1.

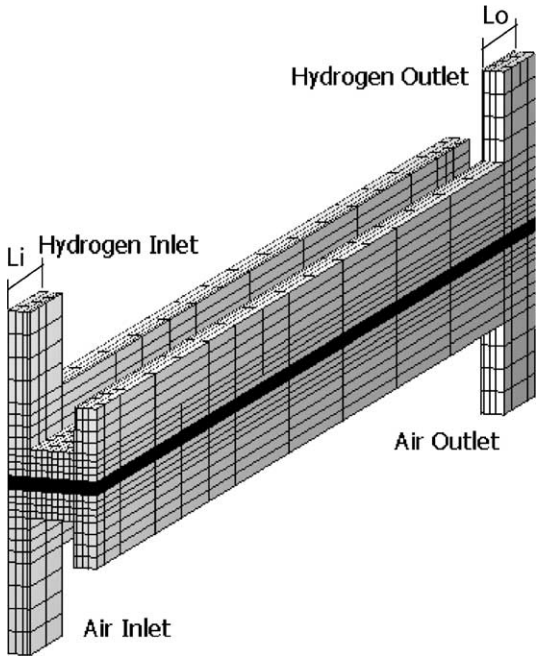

Fig. 2. Isometric view of a fuel cell model with interdigitated channels (500 μm feature size). Only one repeat unit has been modeled to reduce the required computational resources for the calculation.

3.4. Boundary conditions

Gas compositions and their velocities are specified at the gas inlet. The physical information for 30 standard cubic centimeters per minute (sccm) of saturated hydrogen and 80 sccm of saturated air at 50 °C has been assigned to anode inlet and cathode inlet, respectively. A fixed pressure condition (1 atm) is imposed at the gas outlet. The current collection surfaces are assigned with a fixed potential condition. The current density has been obtained by integrating the local current density of these surfaces.

3.5. Solution procedure

A control volume technique has been employed to solve the governing equations with a commercial flow solver

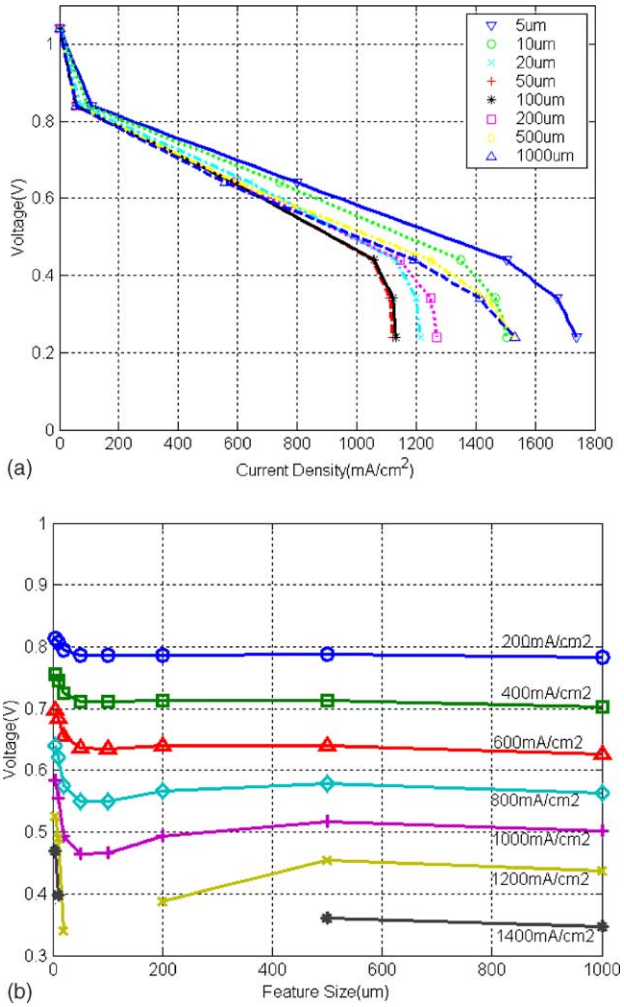

Fig. 3. (a) Model cell polarization curves for the interdigitated flow pattern vs. feature size. Cell electrical performance achieves a maximum at a certain feature size, but increases again for extremely small channels. (b) Here (a) has been rearranged for voltage vs. feature size. At a given constant current density, output voltage peaks around 500 μm feature size. Eventually, it increases again for extremely small (<50 μm).

(CFDRC ver. 2002 from CFD Research Corp.). The details of the procedure are documented elsewhere [23].

4. Scaling observation results

4.1. Interdigitated channels

Fig. 2 shows a fuel cell geometry with interdigitated channels that was generated for the scaling investigation. Only half of the unit pair of inlet and outlet flow channel along the flow direction has been modeled because of the periodic geometry of the interdigitated channels. This simplification significantly reduces the demand for computational resources. Symmetry boundary conditions have been applied to the boundaries facing the repeating units. The flow inlet and outlet have been assumed to be normal to the flow channels. The feature size of the model has been varied between 5 and 1000 μm to investigate the scaling effects over this range.

The cell polarization curves are presented in Fig. 3(a). Interestingly, cell performance increases until the feature size is reduced to 500 μm, but below this feature size, performance starts to *decrease* with the continued the feature size reductions. However, this trend is inversed again as the feature size reaches 50 μm and below. This phenomena can be more clearly observed in Fig. 3(b). It is reported that in parallel channels higher flow velocities in smaller channels induce greater convective mass transport to increase fuel cell performance [8–10]. However, for interdigitated channels, a certain range of feature sizes at the microscale exhibits degraded performance. Thus, in the case of interdigitated channels, scaling down the channel size does not accommodate improved performance except for extremely small channels (<50 μm). In addition, since small channels may suffer from flooding, we may not expect improved performance by scaling down interdigitated flow channels even at extremely small scales [9,10]. Fig. 4 shows the peak power density for each feature size. As expected, the peak power maxes out around 500 μm, reaches minimum at 50 μm, then increases again. Further examination of the oxygen concentration in the cathode reveals a possible explanation for this observation (Fig. 5). Since the flow will have to travel through an electrode and catalyst layer, the oxygen concentration tends to drop across the rib in large-scale channels, e.g. 500 μm channels (Fig. 5(a)). However, smaller ribs maintain more uniform oxygen concentration as the feature size decreases (Fig. 5(b)). Therefore, we may expect improved performance for smaller ribs, which was verified for the case of a 2-D interdigitated channel model [24]. This explains the performance increase between 500 and 1000 μm feature size. However, as the feature size decreases further, the flow along the channel direction is impeded. This effect is more amplified by the dead-ending of interdigitated channels. Thus, the gas preferentially flows through the diffusion layer. This flow pattern causes the decrease of oxygen concentration near the air outlet (Fig. 5(b)). Therefore, the active area near the outlet is not efficiently used. Fig. 6 confirms this analysis. This phenomena results in performance degradation in smaller channels. In contrast to this 3-D modeling result, 2-D models predict a monotonic increase in performance with decreasing feature size [24]. Accordingly, we may conclude that the performance decrease observed between 50 and 500 μm is caused by the

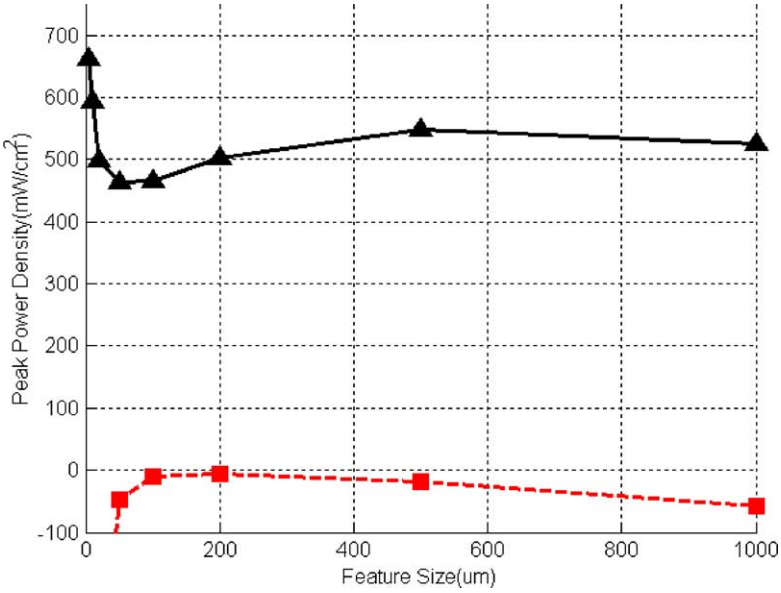

Fig. 4. Peak power density of interdigitated flow channels vs. feature size (▲) and the pressure drop in the flow channels (■). The peak power achieves a maximum at a feature size close to 500 μm. Due to the high pressure drop and the effect of dead end channels, scaling-down interdigitated flow channels does not result in same degree of improvement in performance as with parallel channels [8–10].

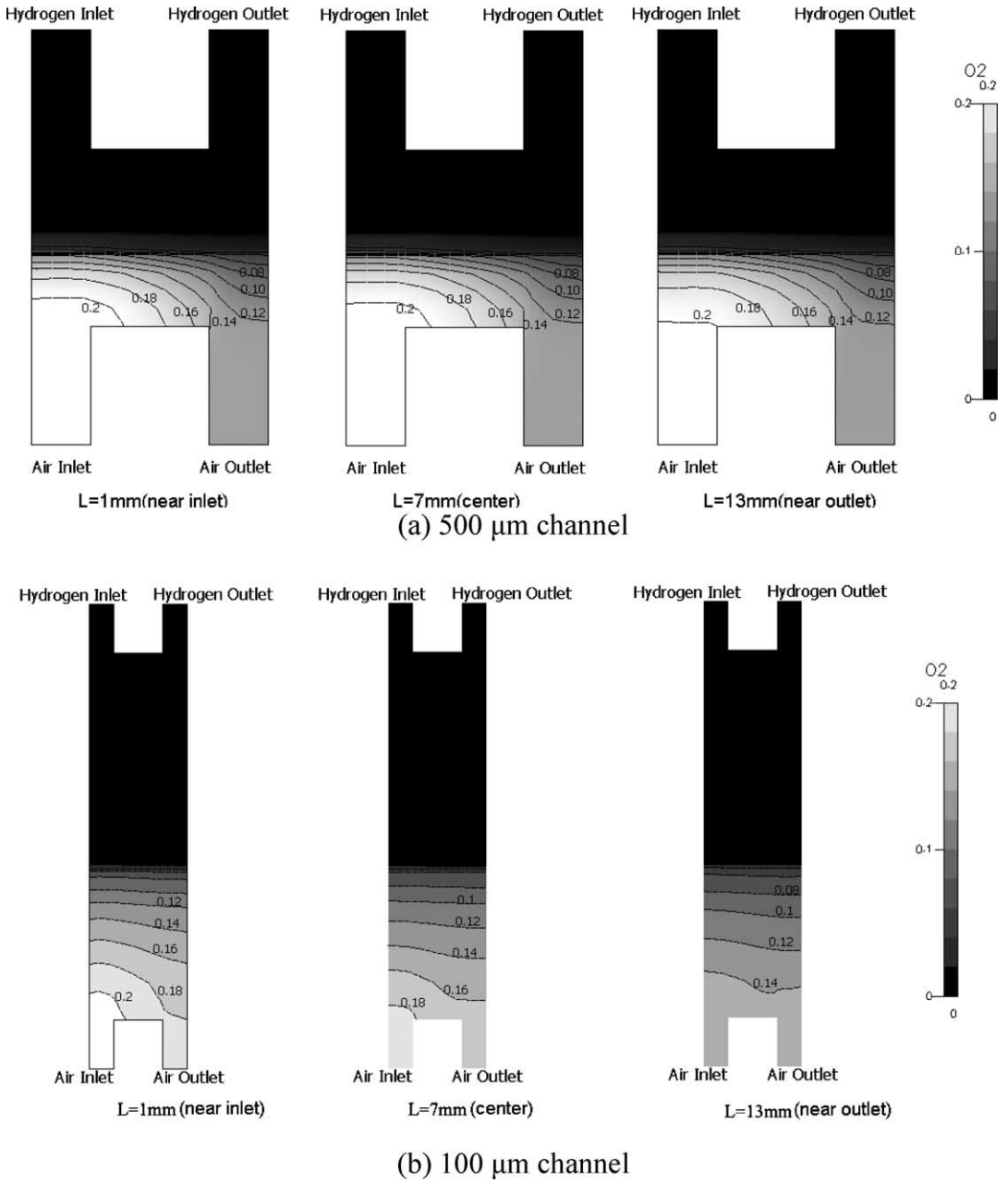

Fig. 5. Oxygen concentration at the cathode at 0.8 V overvoltage. Each picture represents the cross-sectional view at different locations along flow channels. Small channels (b) exhibit more uniform oxygen distribution under the ribs. However, due to the continuous consumption of oxygen at the cathode along the length of its path through the flow channel, oxygen concentration drops near the air outlet. Overall, the performance decreases in small channels.

dead-wall configuration of interdigitated channels, which can be observed in a 3-D model only. In Fig. 7, the current density distribution shows good correlation with the oxygen concentration distribution, confirming the performance difference results from the oxygen concentration distribution.

In Fig. 4, the pressure drop on the cathode side obtained from the model has been plotted along with peak power density. The pressure drop has been converted to power density by following relation:

$$W\,(\mathrm{W/cm^2}) = \frac{P\,(\mathrm{Pa}) \times A_\mathrm{f}\,(\mathrm{m^2}) \times V\,(\mathrm{m/s})}{A_\mathrm{a}\,(\mathrm{cm^2})} \quad (3)$$

where W, P, A_f , V, and A_a represent the pressure drop loss, the pressure drop between the gas inlet and outlet, the cross-sectional flow inlet area, the fluid velocity at the inlet, and the active area, respectively. The pressure drop trend in interdigitated channels is quite unique since for

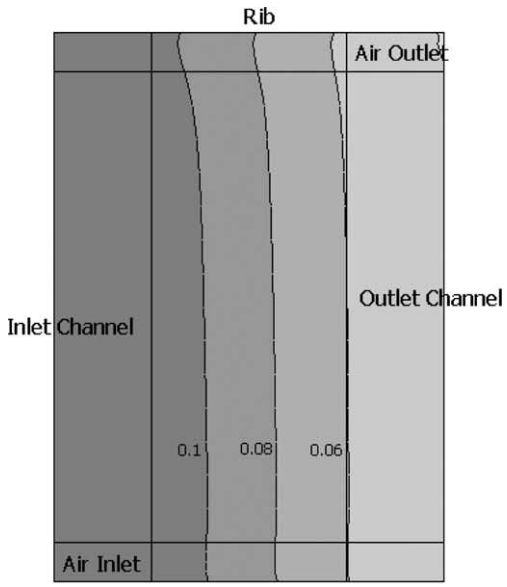

(a) 500 μm channel

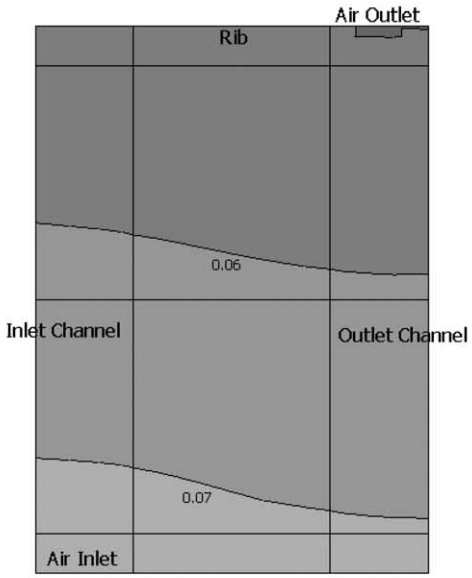

(b) 100 μm channel

Fig. 6. Oxygen concentration at the interface between the catalyst and the gas diffusion layer of the cathode at 0.8 V overvoltage. The pictures has been magnified horizontally since the original picture is relatively narrow. As observed in Fig. 4, the significant change of the oxygen concentration occurs between the inlet channel and the outlet channel for 500 μm channels. However, in 100 μm channels, oxygen concentration changes along the channel direction between the gas inlet and outlet.

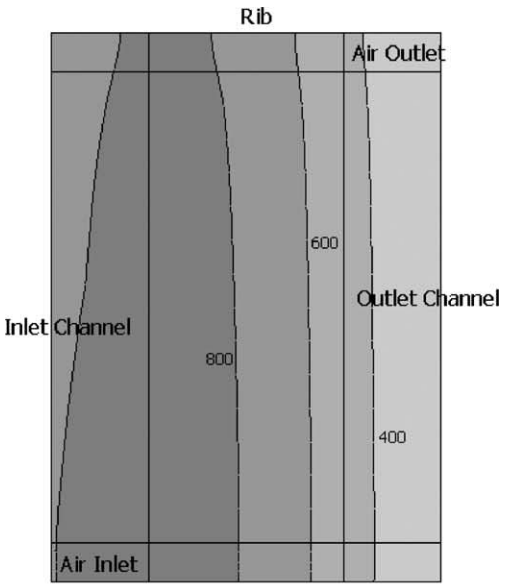

(a) 500 μm channel

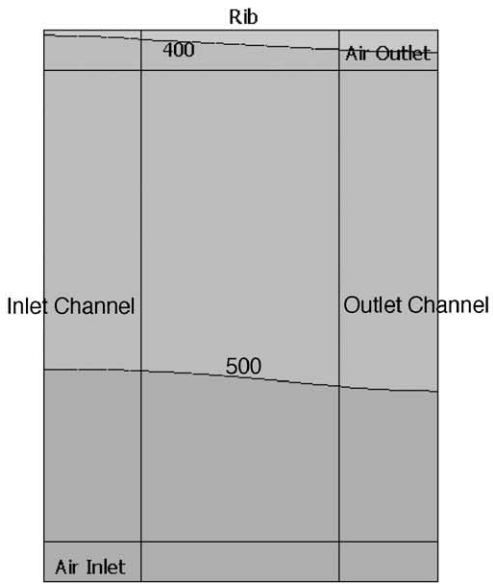

(b) 100 μm channel

Fig. 7. Current density distribution at the same surface shown in Fig. 6. The current density distribution shows a good correlation with the oxygen concentration. 500 μm channels exhibit higher current density.

most other flow channels designs, pressure drop simply increases as channel size decreases [8–10]. The pressure drop of interdigitated channels *decreases* as the feature size decreases to a certain feature size, and then it increases again with decreasing feature size. As the rib size decreases, the path length that gas travels through the diffusion layer decreases. This results in a *decrease* in the pressure drop. However, the decrease in channel size will *increase* the pressure drop. The combination of these two effects results in the trends shown in Fig. 4. It should be noted that the pressure drop loss exceeds the increase of peak power in extremely small channels (<50 μm). This suggests that the increase of the peak power for extremely small channels does not result improved convection but, possibly from the increased pressure in the cathode. The optimum feature size has to be carefully determined considering all the factors mentioned above.

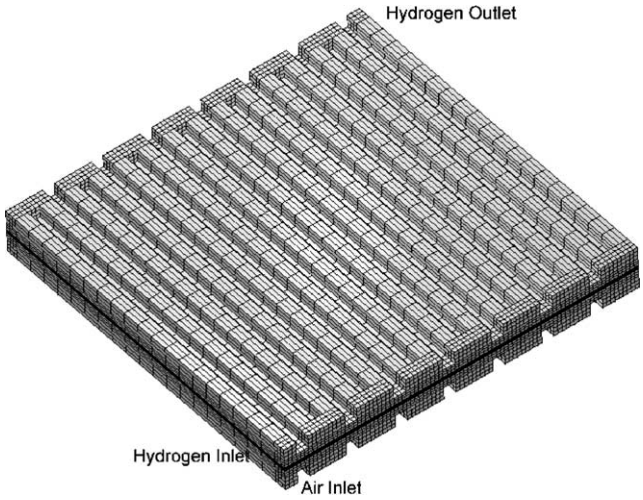

Fig. 8. An isometric view of a fuel cell model with serpentine channels (483 μm feature size). Since no repetitive units exist, entire physical domain has been modeled.

4.2. Serpentine channels

An example serpentine flow channel model is shown in Fig. 8. An important differentiation regarding flow scaling exists between serpentine channels and interdigitated channels. For interdigitated channels, the flow velocity in an individual channel is inversely proportional to the feature size as discussed earlier. However, for serpentine channels, the flow velocity is inversely proportional to the square of feature sizes, since the number of channels is invariant regardless of feature sizes. This relation suggests that the improved convective transport from the scaling effect may be more prominent than for other flow patterns (e.g. parallel or interdigitated channels). Fig. 9(a) and (b) support this idea. The polarization curves of serpentine channels show similar scaling behavior compared to parallel channels [8,10]. However, the performance gain between 483 and 99 μm feature size is larger for serpentine channels (Fig. 10). This result confirms our expectation of the scaling behavior differences. For a better understanding of this issue, it is worthwhile to examine the oxygen distribution in the serpentine channel as shown in Fig. 11. As the channels size decreases from 483 to 99 μm, the oxygen distribution becomes more uniform under the ribs. A similar result has been observed for parallel channels [10]. Accordingly, we may conclude that the increased performance in smaller serpentine channels is due to the increased convection and the reduced dead zone, similar to the case for parallel channels [10]. However, it should be noted that the pressure drop associated with scaling down is much higher for serpentine channels. As explained earlier, one reason is that for serpentine patterns, flow velocity scales with the *square* of the feature size. Another reason is that the channel length is inversely proportional to the feature size (in contrast, the channel length does not vary with feature

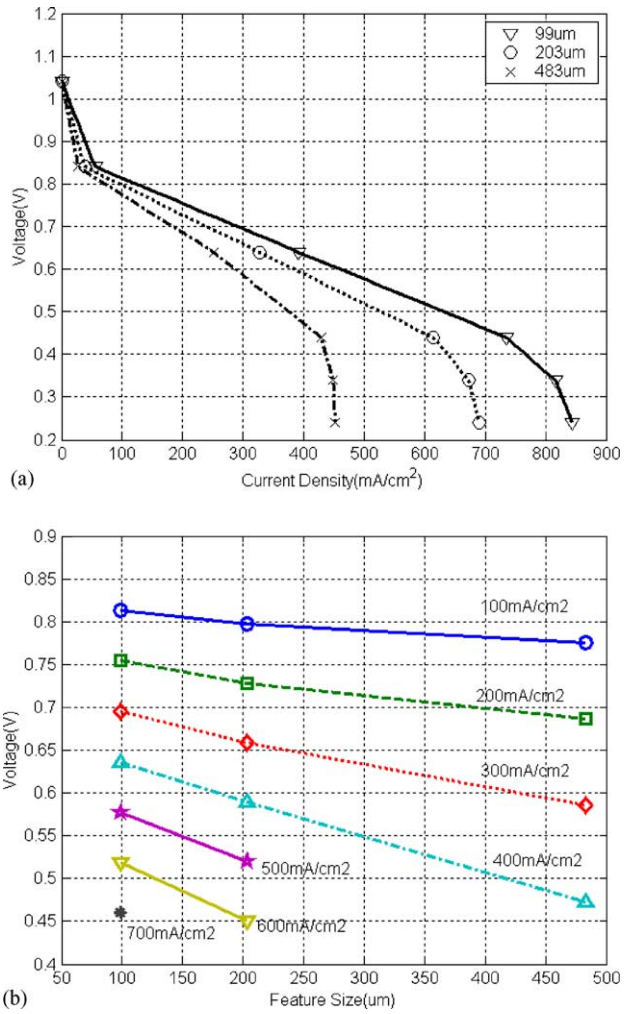

Fig. 9. (a) Model cell polarization curves of serpentine flow channels at various feature sizes. Cell performance increase as the feature size decreases, similar to the trend for parallel channels, although the performance increases in serpentine channels are much more significant compared to parallel channels [8]. (b) Cell polarization curves rearranged for voltage vs. feature size. At a given constant current density, the output voltage increases as the feature size decreases.

sizes for interdigitated or parallel channels). The combined effect of these two scaling behaviors can severely increase the pressure drop in scaled-down serpentine channels. As shown in Fig. 10, pressure loss in 99 and 203 μm channel is so large that it almost negates (or exceeds) the peak power gain from down-scaling. Accordingly, proper care must be taken to determine the optimal channel size.

A comparison of Fig. 12(a) and (b) highlights intriguing scaling effects on oxygen transport and flow. As the channel size decreases, the higher flow resistance forces a significant portion of the gas to flow directly through the gas diffusion layer instead. The appearance of this short-cut results in poor convection in certain areas, such as the dotted area shown in Fig. 12(b). Such areas tend to suffer from oxygen deficiency. Fig. 13 reveals that the current density in

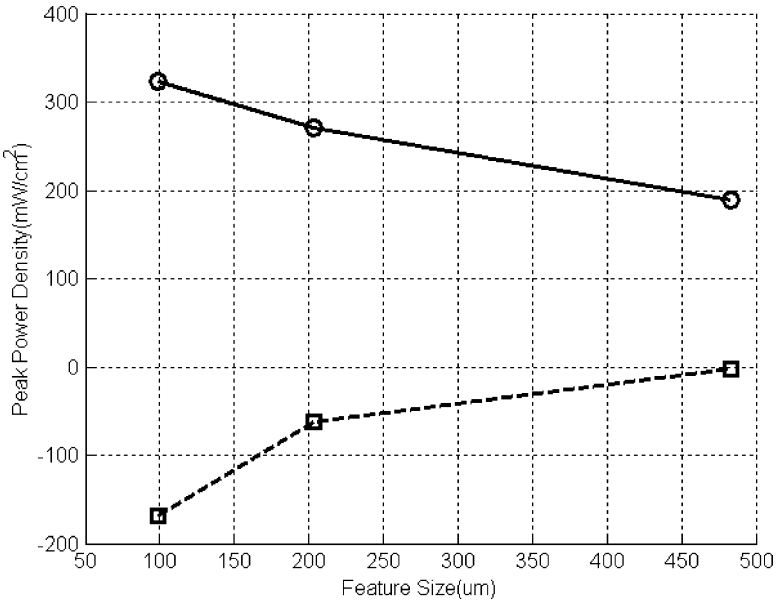

Fig. 10. The peak power density of serpentine flow channels (○) and the pressure drop in the flow channels (□). Even though the peak power density gain is larger compared to parallel channels with the decreasing feature size, the associated power loss from the pressure drop exceeds the gain [8].

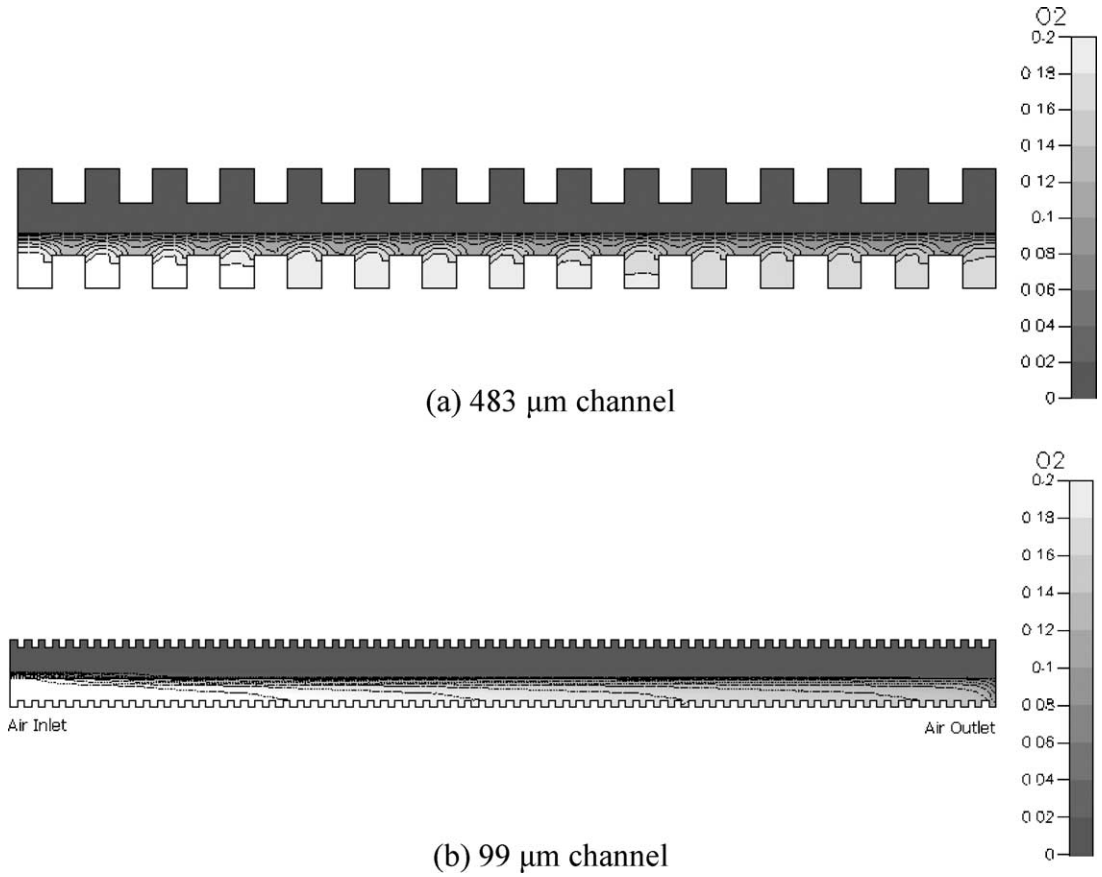

Fig. 11. Oxygen concentration in the cathode at 0.8 V overvoltage. In this figure, the cross-section of the serpentine channel is shown at the center along the straight portion of the channels ($L = 7$ mm). A smaller channel (99 μm) exhibits more uniform oxygen distribution under the dividing ribs. Also, the concentration gradually decreases from high near the inlet region (left) to low near the outlet region (right). However, in large channels (483 μm), significant rib dead zones appear.

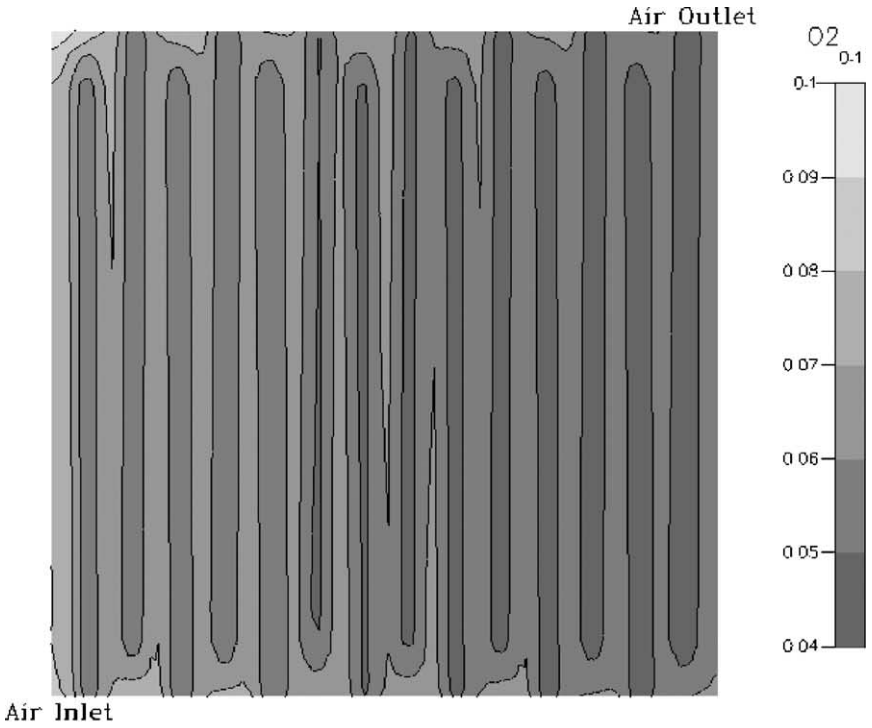

(a) 483 μm channel

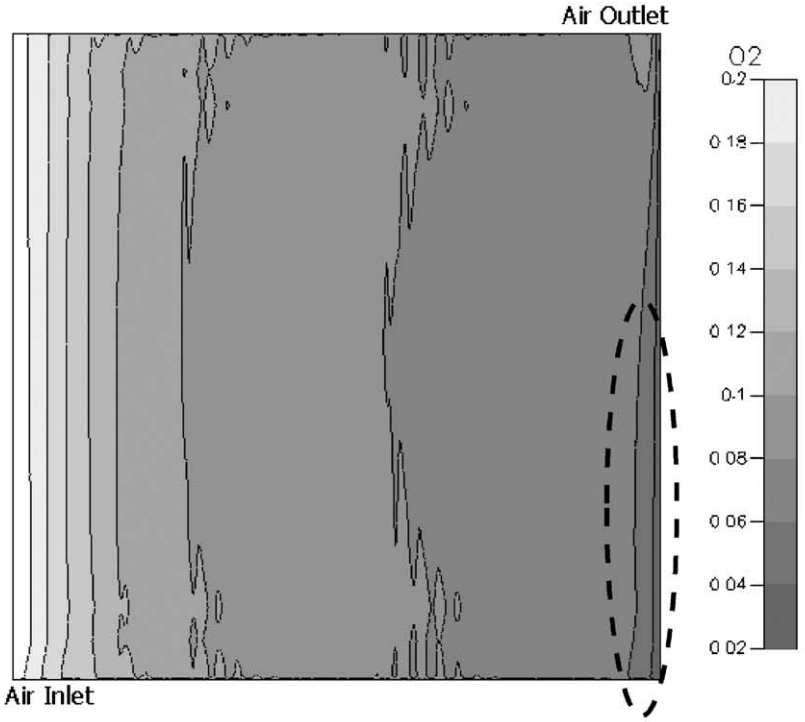

(b) 99 μm channel

Fig. 12. Oxygen concentration at the interface between the catalyst and the gas diffusion layer of the cathode at 0.8 V overvoltage. (a) In large channels, oxygen deficiency under the rib is prominent. (b) Due to the high pressure drop in the small channel, the flow does not fully reach bottom right corner (dotted region).

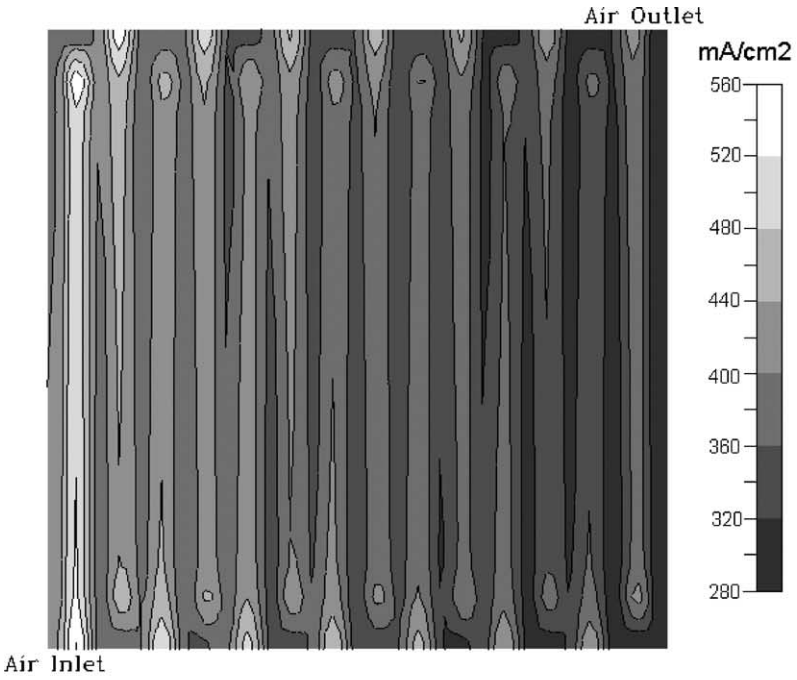

(a) 483 μm channel

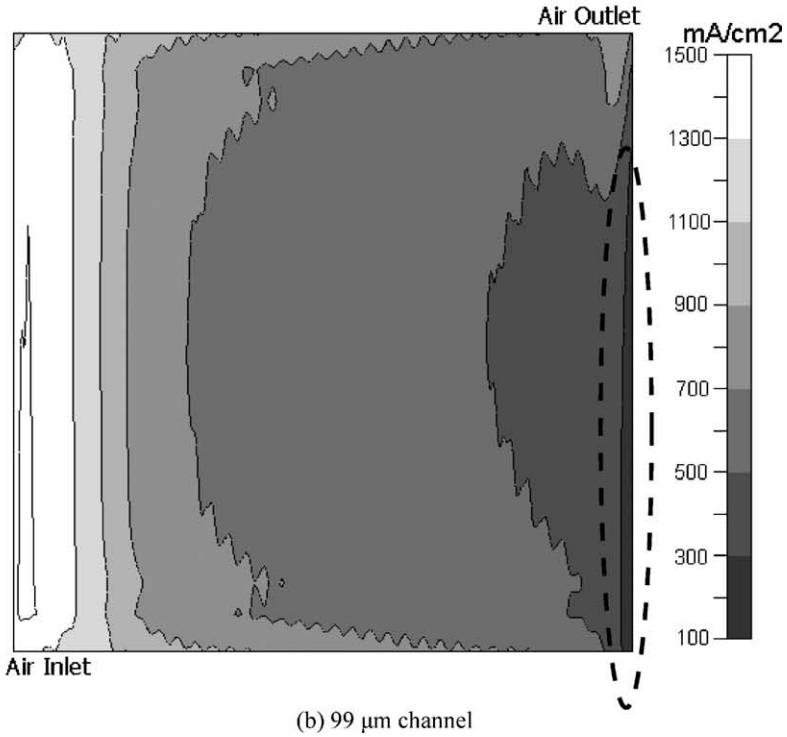

(b) 99 μm channel

Fig. 13. Current density distribution at the surface shown in Fig. 12(a). In large channels, the locations of ribs are noticeable since the current density under the ribs are higher than that of the surroundings. (b) In small channels, the oxygen deficient region shown in Fig. 12 (dotted area) exhibits lower current density.

this oxygen deficient area is lower than other areas. Therefore, the active area is not fully utilized due to the inefficient flow routing. This effect may be even more severe in PEM fuel cells than the simulation suggests, since liquid water will increase the pressure drop even further. (Please remember liquid water is not considered in our model.) Additionally, this dead-corner region is more prone to suffer from bulk flooding, since liquid water can build up easily in the absence of forced flow. In the same context, the gas inlets and outlets must be located on opposite sides of the cell to

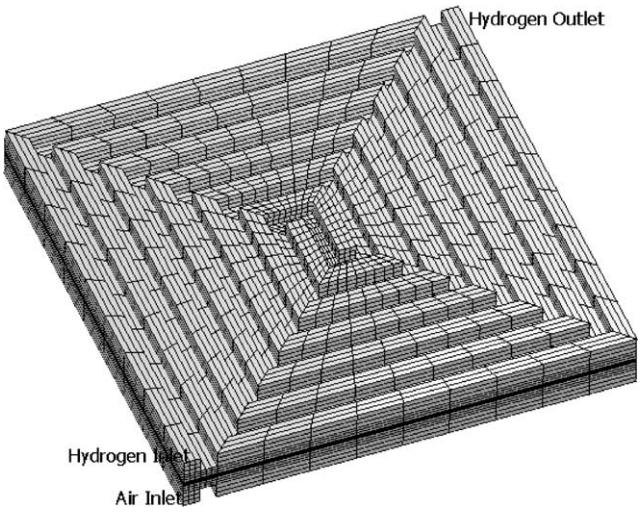

Fig. 14. Isometric view of the fuel cell model with serpentine-interdigitated channels (510 μm feature size). A single pair of flow channels exists, which are connected to the inlet and the outlet, respectively. The gas flow will travel from the inlet side channel to outlet side channel through the gas diffusion layer.

minimize unused active area. It should be noted that in actual fuel cell operations, even relatively large flow channels may exhibit similar behavior to microscale channels, including flow short-circuits and liquid water build-ups.

4.3. Spiral-interdigitated channels

As shown previously, interdigitated channels have the highest performance due to forced convection in the gas diffusion layer. Multiple flow channels, or flow paths, exist between inlet and outlet, thus in actual fuel cell

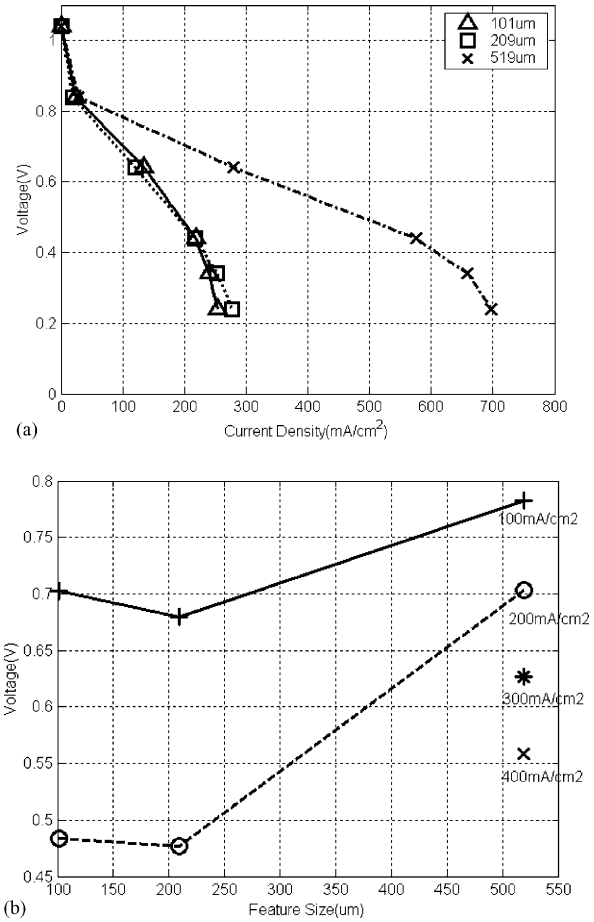

Fig. 15. (a) Model cell polarization curves of the spiral-interdigitated channels at various feature sizes. Cell electrical performance decreases as the feature size decreases. (b) (a) has been rearranged for voltage vs. feature size. A slight increase of performance is observed from 209 to 101 μm channel size.

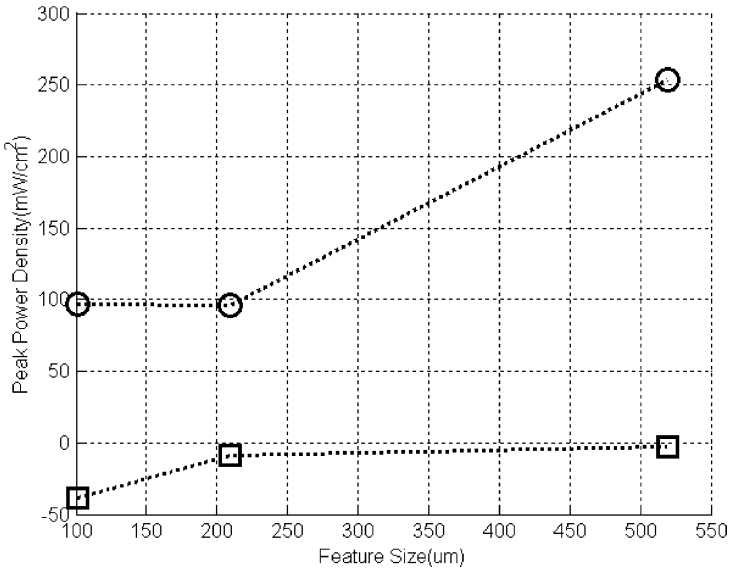

Fig. 16. Peak power density of spiral-interdigitated channels (○) and the pressure drop in the flow channels (□). The peak power density decreases as the feature size decreases, even though the slight increase of power density is observed from 209 to 101 μm, which mainly comes from the pressure drop effect.

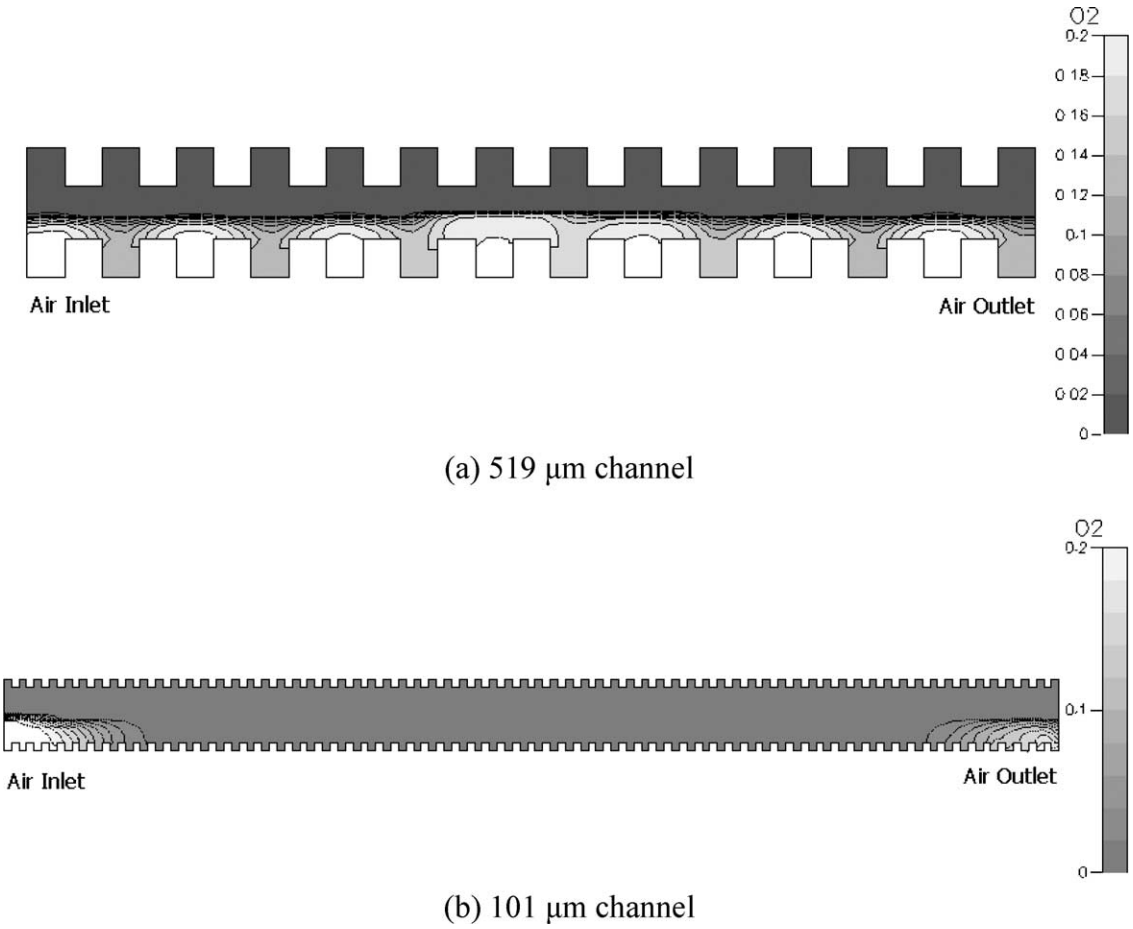

Fig. 17. Oxygen concentration of the cathode at 0.8 V overvoltage shown at the cross-section ($L = 7$ mm). (a) In 519 μm channels, oxygen concentration in channels near the center of the active area is not much different from the concentration in channels near the inlet or outlet. (b) In 101 μm channels, the disappearance of the dead zone under ribs is observed similar to the other flow patterns. However, the oxygen is completely depleted at the center of the active area due to the short-circuiting of flow path.

operation certain channels may not be functional due to unstable flow routing or flooding [25]. In contrast, serpentine channels have the advantage of a single flow routing path, leading to better reactant removal. Combining the advantages of the two flow patterns, a new flow pattern can be proposed as shown in Fig. 14. In this flow pattern—henceforth called the "spiral-interdigitated" flow pattern—a single inlet and outlet channel exist, similar to serpentine channels. However, these inlet and outlet channels are discontinuous, which ensures forced convection through the gas diffusion layer. Thus, we may expect improved performance while still maintaining good reactant removal capability.

Fig. 15 shows the cell polarization curves for a series of spiral-interdigitated patterns. As expected, the performance of 510 μm spiral-interdigitated channels is better than that of 483 μm serpentine channels (refer back to Fig. 9). However, the scaling behavior is quite different from that of serpentine channels. Considering the losses due to pressure drops as shown in Fig. 16, the peak power density of the spiral-interdigitated cell decreases as the feature size decreases over the investigated range. A slight increase in the peak power density is observed in scaling down from 209 to 101 μm, but this performance gain comes from the pressure drop as shown in Fig. 16. Thus, the scaling behavior of the spiral-interdigitated channel is more like that of interdigitated channels. Details of the oxygen concentration distribution in spiral-intedigitated channels explain the scaling behavior as shown in Figs. 17 and 18. In small channels, the disappearance of the dead zone under ribs is observed just like in other flow patterns (Fig. 17(b)). However, the flow path short-circuits are highly prominent in the smaller channels. In Figs. 17(b) and 18(b), the oxygen is completely depleted at the center of the active area due to the high pressure drop in the flow channels. The flow only travels along the edge of the active area, and directly reaches outlet through the gas diffusion layer. Similar behavior has previously been observed in serpentine channels. The down-scaling of spiral-interdigitated channels may not be favorable (Fig. 19).

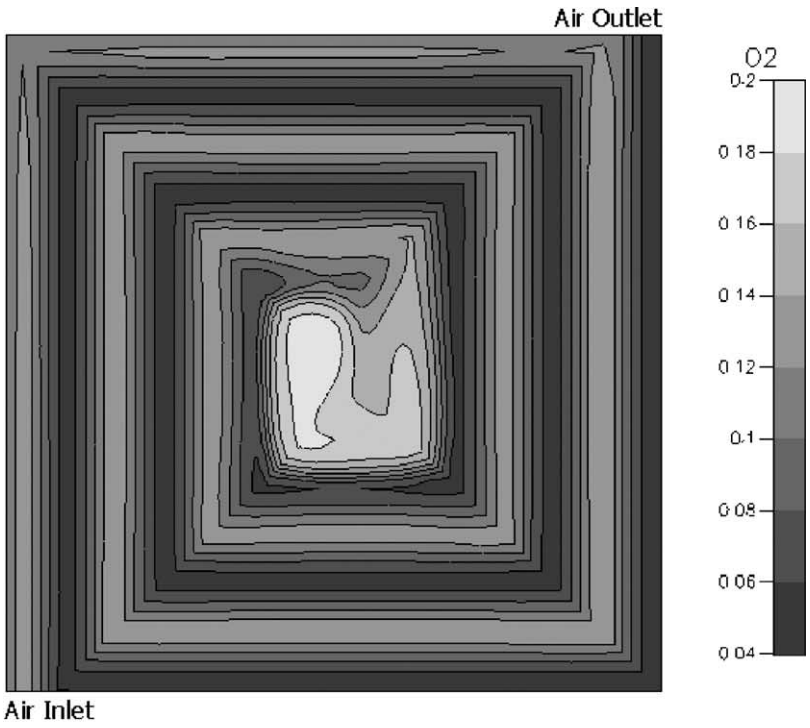

(a) 519 μm channel

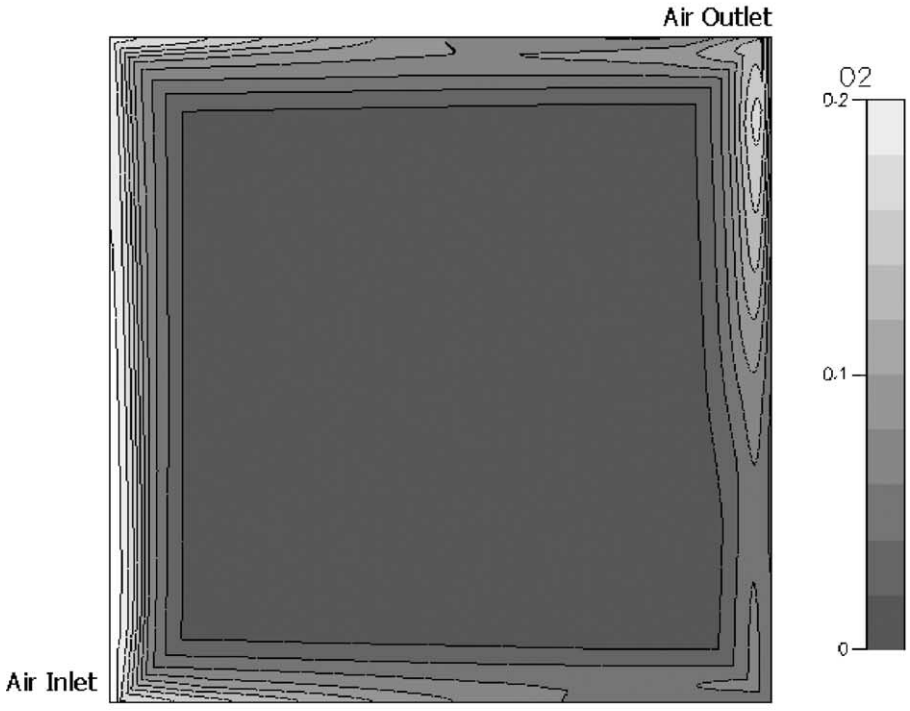

(b) 101 μm channel

Fig. 18. Oxygen concentration at the interface between the catalyst and the gas diffusion layer of the cathode at 0.8 V overvoltage. (a) Similar to other flow patterns with large channels, dead-zones under the ribs are observed. (b) Due to the high pressure drop in the small channels (101 μm), the air flow travels only edge of the active area, and directly goes to the outlet through the gas diffusion layer before reaching the center of the active area.

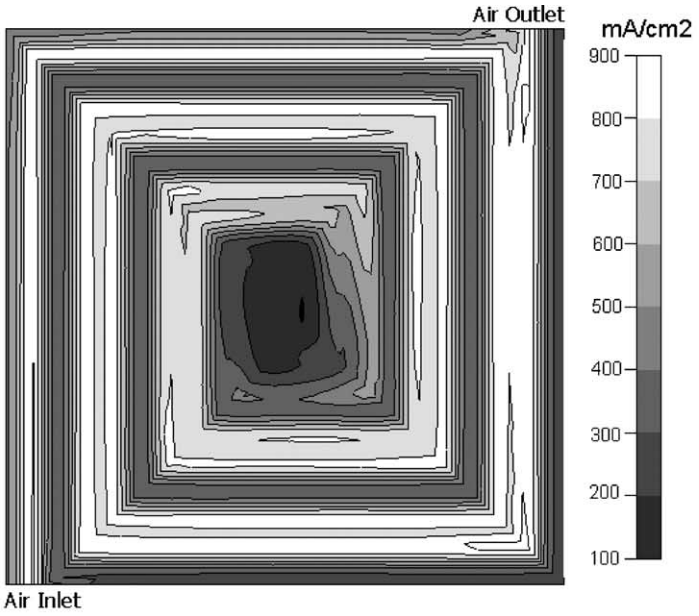

(a) 519 μm channel

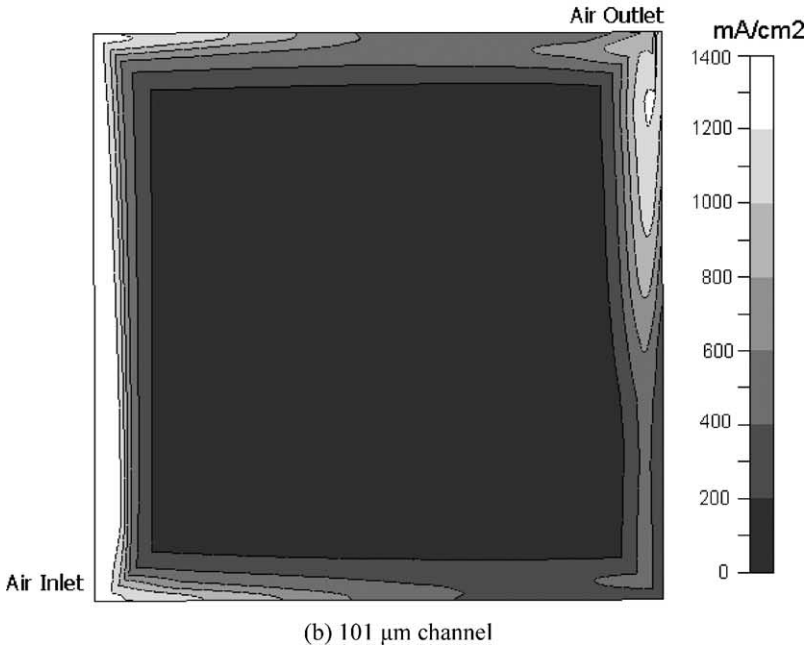

(b) 101 μm channel

Fig. 19. Current density distribution at the same surface shown in Fig. 18. The current density distribution shows a good correlation with the oxygen concentration shown in Fig. 18. The edges of the active area of small channel (101 μm) exhibit higher current density than large channel (519 μm). However, the overall current density of small channel is lower since the relatively large area in the center generates extremely low current density.

5. Conclusion

We have presented observations on the scaling effects of various flow channels in fuel cells with gaseous hydrogen/air reactants.

A three-dimensional computational model of serpentine channels predicts that microchannels (<100 μm) may not be favorable due to high pressure drops in spite of large performance gains arising from scaling down the flow channels. In addition, flooding may impose an adverse effect in microchannels [10]. A good compromise, however, can be achieved by employing parallel-serpentine flow patterns for certain feature size regions.

Interdigitated channels exhibited excellent performance results based on the model. Their scaling behavior is quite complicated due to highly non-linear convection both in the flow channels and the porous electrode. Considering the model predictions, flooding issues, and pressure drop losses,

the performance of interdigitated channels decreases as the feature size decreases. In addition, the relatively high pressure drop in interdigitated channels may cause difficulties for its option in miniature fuel cells due to the increase load of auxiliary devices, such as pump systems. A good compromise may be found between reduced pressure drop and reduced performance at intermediate feature sizes depending on operation requirements.

A new type of flow pattern—the spiral-interdigitated pattern—has been proposed to combine the advantages of interdigitated channels and serpentine channels. In the conventional scale, the spiral-interdigitated pattern exhibits promising results compared to serpentine channels. But, the scaling behavior is similar to that of interdigitated channels, indicating that they may not be effective at small scale.

The effect of scaling down the feature size of flow channels is complex, depending strongly on the fuel cell geometry and operating conditions. Based on the observations presented in this work, we conclude that the adoption of micro flow channels in fuel cells requires careful consideration of the geometric effects (e.g. interdigitated channels) and flooding issues [10]. However, this conclusion may be valid only for the geometry of active area ($14\,\text{mm} \times 14\,\text{mm}$) investigated in this paper. If a much smaller or differently shaped active area is employed, the optimum feature size could vary. Also, certain operating environments may be more favorable for microchannels, e.g. using dry air would retard flooding, a situation that is probable in miniature fuel cells with simplified auxiliary devices [8].

In future designs, the employment of microchannels still offers opportunities to improve performance. For example, the incorporation of novel water removal mechanisms, such as capillary or electrokinetic pumps is possible, both of which are more efficient of the micro scale. Also, extremely thin diffusion layers with reduced dead zone will increase the diffusion limit significantly, making microchannels attractive. These studies are left for future work.

Acknowledgements

This work was sponsored by Stanford University, a Stanford Graduate Fellowship, and Honda R&D Co. Ltd.

References

[1] C.K. Dyer, J. Power Sources 106 (2002) 31.
[2] G.J.K. Acres, J. Power Sources 100 (2001) 60.
[3] P. Costamagna, S. Srinivasan, J. Power Sources 102 (2001) 253.
[4] A. Heinzel, C. Hebling, M. Muller, M. Zedda, C. Muller, J. Power Sources 105 (2002) 250.
[5] S.C. Kelley, G.A. Deluga, W.H. Smyrl, Electrochem. Solid State 3 (2000) 407.
[6] S.J. Lee, A. Chang-Chien, S.W. Cha, R. O'Hayre, Y.I. Park, Y. Saito, F.B. Prinz, J. Power Sources 112 (2002) 410.
[7] R. O'Hayre, D. Braithwaite, W. Herman, S.J. Lee, T. Fabian, S.W. Cha, Y. Saito, F.B. Prinz, J. Power Sources 124 (2003) 459.
[8] S.W. Cha, S.J. Lee, Y.I. Park, F.B. Prinz, Fuel cell science, engineering, and technology, in: R.K. Shah, S.G. Kandlikar (Eds.), Proceedings of First International Conference on Fuel Cell Science, Engineering, and Technology, ASME, NY, 2003, p. 143.
[9] S.W. Cha, R. O'Hayre, F.B. Prinz, Materials for energy conversion and environment, in: Proceedings of 14th International Conference on Solid State Ionics, Monterey, CA, 2003.
[10] S.W. Cha, R. O'Hayre, S.J. Lee, Y. Saito, F.B. Prinz, J. Electrochem. Soc., in press.
[11] R. O'Hayre, S.J. Lee, S.W. Cha, F.B. Prinz, J. Power Sources 109 (2002) 483.
[12] V. Gurau, S. Kakac, H. Liu, ASME Adv. Energy Syst. Div. Publ. AES 38 (1998) 205.
[13] W. He, J.S. Yi, T.V. Nguyen, AIChE J. 46 (2000) 2053.
[14] D. Natarajan, T.V. Nguyen, J. Electrochem. Soc. 148 (2001) A1324.
[15] S. Um, C.Y. Wang, K.S. Chen, J. Electrochem. Soc. 147 (2000) 4485.
[16] Z.H. Wang, C.Y. Wang, K.S. Chen, J. Power Sources 94 (2001) 40.
[17] A. Kumar, R.G. Reddy, J. Power Sources 113 (2003) 11.
[18] H.N. -Neshat, S. Shimpalee, S. Dutta, W.K. Lee, J.W. Van Zee, ASME Adv. Energy Syst. Div. Publ. AES 39 (1999) 337.
[19] S. Dutta, S. Shimpalee, J.W. Van Zee, J. Appl. Electrochem. 30 (2000) 135.
[20] S. Dutta, S. Shimpalee, J.W. Van Zee, Int. J. Heat Mass Transfer 44 (2001) 2029.
[21] W.M. Kays, M.E. Crawford, Convective Heat and Mass Trasnfer, third ed., McGraw-Hill, NY, 1993.
[22] T.E. Springer, T.A. Zawodzinski, M.S. Wilson, S. Gottesfeld, J. Electrochem. Soc. 143 (1996) 587.
[23] CFD-ACE(U)^{TM} User Manual, CFD Research Corp., Huntsville, AL, 2002.
[24] J.S. Yi, T.V. Nguyen, J. Electrochem. Soc. 146 (1999) 38.
[25] T.V. Nguyen, M.W. Knobbe, J. Power Sources 114 (2003) 70.